Histone Sprocket Arginine Residues Are Important for Gene Expression, DNA Repair, and Cell Viability in *Saccharomyces cerevisiae*

Amelia J. Hodges,[1] Isaura J. Gallegos,[1] Marian F. Laughery, Rithy Meas, Linh Tran, and John J. Wyrick[2]
School of Molecular Biosciences and Center for Reproductive Biology, Washington State University, Pullman, Washington 99164

ABSTRACT A critical feature of the intermolecular contacts that bind DNA to the histone octamer is the series of histone arginine residues that insert into the DNA minor groove at each superhelical location where the minor groove faces the histone octamer. One of these "sprocket" arginine residues, histone H4 R45, significantly affects chromatin structure *in vivo* and is lethal when mutated to alanine or cysteine in *Saccharomyces cerevisiae* (budding yeast). However, the roles of the remaining sprocket arginine residues (H3 R63, H3 R83, H2A R43, H2B R36, H2A R78, H3 R49) in chromatin structure and other cellular processes have not been well characterized. We have genetically characterized mutations in each of these histone residues when introduced either singly or in combination to yeast cells. We find that pairs of arginine residues that bind DNA adjacent to the DNA exit/entry sites in the nucleosome are lethal in yeast when mutated in combination and cause a defect in histone occupancy. Furthermore, mutations in individual residues compromise repair of UV-induced DNA lesions and affect gene expression and cryptic transcription. This study reveals simple rules for how the location and structural mode of DNA binding influence the biological function of each histone sprocket arginine residue.

KEYWORDS nucleotide excision repair; cryptic transcription; nucleosome; histone assembly

THE histone octamer, which is composed of two copies each of histones H2A, H2B, H3, and H4, binds with high affinity to ~147 bp of DNA to form the nucleosome core particle. Histone-DNA binding is mediated by >100 histone main-chain and side-chain interactions with the DNA sugar-phosphate backbone and a similar number of indirect water-mediated interactions (Davey *et al.* 2002; Muthurajan *et al.* 2003). These interactions occur primarily at 14 locations in the nucleosome structure where the DNA minor groove faces the histone octamer [superhelical locations (SHL) −6.5 to 6.5] (Luger *et al.* 1997). At each of these locations, an arginine side chain extends into the DNA minor groove and makes extensive contacts with the DNA backbone (Figure 1A).

We will refer to the arginine residues that insert into the DNA minor groove as "sprocket" arginines, since they engage the DNA "chain" like the teeth of a bicycle sprocket wheel. Sprocket arginine residues are highly conserved (Muthurajan *et al.* 2003; Sullivan and Landsman 2003), and the insertion of sprocket arginine side chains into the DNA minor groove comprises a significant fraction of the solvent accessible surface area that is buried upon histone-DNA binding (Davey *et al.* 2002). Studies have suggested that sprocket arginine–DNA contacts may play an important role in the rotational positioning of nucleosomes (Luger *et al.* 1997; Harp *et al.* 2000; Rohs *et al.* 2009; Wang *et al.* 2010; West *et al.* 2010). For example, short poly(A) stretches narrow the DNA minor groove, potentially enhancing electrostatic interactions between the DNA phosphate backbone and the sprocket arginine (Rohs *et al.* 2009; West *et al.* 2010).

While sprocket arginine residues appear to have unique and important roles in DNA binding and are highly conserved among eukaryotic species, mutational screens in yeast revealed that only one of these arginine residues, H4 R45, is essential for cell viability (Matsubara *et al.* 2007; Dai *et al.* 2008; Nakanishi *et al.* 2008) (Figure 1B). H4 R45 contacts the DNA at superhelical locations flanking the dyad (SHL ±0.5) and is lethal when

doi: 10.1534/genetics.115.175885
Manuscript received February 25, 2015; accepted for publication May 4, 2015; published Early Online May 12, 2015.
Supporting information is available online at www.genetics.org/lookup/suppl/doi:10.1534/genetics.115.175885/-/DC1.
[1]These authors contributed equally to this work.
[2]Corresponding author: School of Molecular Biosciences, Biotechnology Life Sciences 241, Washington State University, Pullman, WA 99164.
E-mail: jwyrick@vetmed.wsu.edu

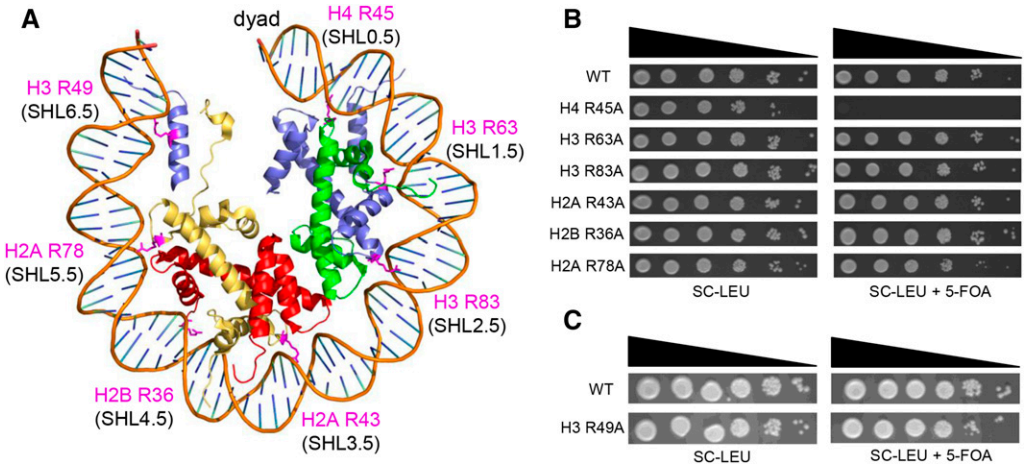

Figure 1 Growth phenotypes of single sprocket arginine histone mutants. (A) Location of the sprocket arginine residues is highlighted in pink in the yeast nucleosome structure (1id3) (White *et al.* 2001). (B and C) Yeast strains containing a single histone arginine mutation were spotted at decreasing serial dilutions on SC-LEU and SC-LEU +5-FOA plates. The SC-LEU+5-FOA plates select against a *URA3* plasmid containing wild-type histones, revealing the growth phenotype of the histone mutant. SHL, superhelical location.

mutated to alanine or cysteine (Fry *et al.* 2006; Matsubara *et al.* 2007; Dai *et al.* 2008; Nakanishi *et al.* 2008). It is not clear if H4 R45 is essential because it binds near the dyad, because it binds immediately adjacent SHLs (−0.5 and +0.5), or because it plays some other essential function.

Mutations in the H4 R45 residue (H4 R45C and H4 R45H) were originally isolated from a yeast genetic screen for switch-independent (*sin*) mutants (Kruger *et al.* 1995). Expression of the H4 R45C (or R45H) mutant partially alleviates the requirement for the SWI/SNF remodeling complex to activate the expression of the yeast homothallic switching endonuclease (HO) gene. H4 R45C and R45H mutants also enhance nucleotide excision repair (NER) of UV-induced cyclobutane pyrimidine dimers (CPDs) and render yeast cells more resistant to UV radiation (Nag *et al.* 2008). These effects on transcription and DNA repair appear to be a consequence of how the H4 R45C mutant alters the DNA accessibility, intrinsic mobility, and stability of yeast nucleosomes (Kurumizaka and Wolffe 1997; Wechser *et al.* 1997; Flaus *et al.* 2004; Muthurajan *et al.* 2004). The crystal structure of the H4 R45C mutant nucleosome revealed no significant distortions in the nucleosome structure (Muthurajan *et al.* 2004). Instead, the H4 R45C mutant eliminates stabilizing van der Waals contacts between H4 R45 and the DNA minor groove (Muthurajan *et al.* 2004). The H4 R45C mutant can also affect Mg^{2+}-dependent higher-order folding of nucleosome arrays (Horn *et al.* 2002), indicating that the effects of this mutation may extend beyond the mononucleosome.

Another sprocket arginine residue, H3 R83, was isolated in a genetic screen for mutants that caused the loss of ribosomal DNA (rDNA) silencing (LRS) in yeast (Park *et al.* 2002). The H3 R83A mutant causes recessive defects in rDNA and telomere silencing and a dominant defect in HML silencing (Park *et al.* 2002). The H3 R83A mutant cells are marginally more sensitive to the DNA-damaging agent methyl methanesulfonate (MMS) in some strain backgrounds (Matsubara *et al.* 2007). However, the H3 R83A mutant does not have a *sin* phenotype, nor does it affect Mg^{2+}-dependent higher-order folding of nucleosome arrays (Fry *et al.* 2006), indicating that it has phenotypes distinct from that of the H4 R45 mutants.

Much less is known about the function of the other sprocket arginine residues (H3 R63, H2A R43, H2B R36, H2A R78, and H3 R49). Global screens of histone mutant phenotypes in yeast found that both H3 R49A and H2A R78A mutants have increased sensitivity to hydroxyurea (HU, a DNA replication inhibitor), high temperature (39°), and the DNA-damaging agent MMS (Dai *et al.* 2008; Huang *et al.* 2009; Sakamoto *et al.* 2009; Dai *et al.* 2010). The H3 R49A mutant was also found to be more sensitive to UV radiation (Dai *et al.* 2008; Huang *et al.* 2009) and induces cryptic transcription (Hainer and Martens 2011). The H2A R78A mutant was found to be more sensitive to the DNA-damaging agent camptothecin (Dai *et al.* 2010). One study observed marginal HU and MMS sensitivities for the H3 R63A mutant (Sakamoto *et al.* 2009). In contrast, the H2A R43A and H2B R36A mutants have no apparent phenotype when mutated to alanine (Matsubara *et al.* 2007; Huang *et al.* 2009). The H2B R36 residue is part of the histone H2B repression (HBR) cassette (Parra *et al.* 2006). Deletion of the eight-residue HBR cassette increases the expression of a large fraction of the yeast genome, renders cells more sensitive to UV radiation and other DNA-damaging agents (Parra *et al.* 2006), and affects NER at certain loci (Nag *et al.* 2010). It is not clear whether H2B R36 or other residues in the HBR domain play a functional role in these processes.

In this study, we investigated the role of histone sprocket arginine residues in gene expression, DNA repair, and cell viability. We found that mutants in sprocket arginine residues that contact the distal ends of nucleosomal DNA (*i.e.*, H2A R78 and H3 R49) show enhanced sensitivity to UV radiation, which appears to be due to a defect in NER of UV-induced DNA lesions. In contrast, while these mutants also show enhanced sensitivity to the DNA alkylating agent MMS, we did not observe a corresponding defect in base excision repair (BER). Moreover, our data indicate that the H3 R49A mutant has a unique SIN phenotype, while the H2A R78A mutant derepresses the expression of many genes and causes a defect in telomeric silencing. Additionally, multiple sprocket arginine mutants show enhanced levels of cryptic transcription. Finally, we find that the double

mutants of adjacent sprocket arginines that contact the distal ends of the nucleosomal DNA (*i.e.*, H2A R78A-H3 R49A or H2A R78A-R36A) are lethal in yeast.

Materials and Methods

Yeast strains and plasmids

The yeast strains and plasmids used in this study are described in Supporting Information, Table S1 and Table S2. These strains were derived from strain JHY205 (Ahn *et al.* 2005), which has the chromosomal copies of each canonical histone gene deleted. The sprocket arginine histone mutants were constructed in plasmid pQQ18 (Ahn *et al.* 2005), which contains genes for each of the canonical histones (*i.e.*, *HTA1-HTB1 HHT2-HHF2*). Mutants were constructed by site-directed mutagenesis using a modified version of the QuikChange method and verified by DNA sequencing. The *HO-lacZ* reporter was constructed by first replacing a portion of the *HO* gene with a *URA3* marker, followed by replacement of the *URA3* marker with the *HO-lacZ* construct, which is inserted at position +58 in the *HO* open reading frame. The *FLO8-HIS3* reporter was constructed using the CRISPR/Cas9 system, which will be described in more detail elsewhere. Primer sequences are available upon request. Standard growth conditions, media, and yeast (and *Escherichia coli*) methods were used in strain construction and cell growth.

Yeast growth curves

Growth curves were conducted as previously described (Jin *et al.* 2007). Yeast strains were grown to an optical density at 600 nm (OD_{600}) of 0.01 in selective media containing galactose, permitting the expression of wild-type histones. Cells were then washed with water and resuspended in glucose media, repressing the expression of wild-type histones. Time "0" is defined as the point at which the cells were switched to glucose. OD_{600} measurements were taken at the indicated time points. Growth curves shown are representative of at least three independent replicates.

Yeast spotting

Logarithmically growing yeast strains were spotted as 1:10 serial dilutions onto the indicated media with 2% glucose. For MMS experiments, yeast strains were spotted onto synthetic complete (SC) media containing the indicated doses of MMS (Sigma). Images were taken after 4 days incubation at 30°. For UV experiments, plates were irradiated with the indicated dose of UV light (50, 100, or 150 J/m^2) after spotting onto SC media. Images were taken after 4 days incubation in the dark (*i.e.*, plates wrapped in aluminum foil) at 30°.

Quantitative UV sensitivity assays

To assess UV sensitivity, yeast strains were grown overnight in yeast extract peptone dextrose (YPD) medium to logarithmic phase. Serial dilutions were plated onto YPD plates and irradiated with the indicated dose of UV light (50, 100, or 150 J/m^2). Irradiated plates were wrapped in aluminum foil and incubated at 30° for 2–3 days, after which point the aluminum foil was removed and an initial colony count was made. Plates were allowed to incubate at 30° for up to 2 weeks, and subsequent counts were made every few days, with the majority of colonies appearing by the fourth day. A minimum of three replicates was performed for each strain. Survival was determined by dividing the relative colony-forming units (CFUs) on the irradiated plates by the relative CFUs of plates that were not irradiated.

LacZ assays

LacZ assays were performed as described in the Clontech Yeast Protocols Handbook. Briefly, cells were grown in YPD medium to an OD_{600} of 0.4–0.9. The cells were pelleted, washed, and then resuspended with Z buffer (60 mM $Na_2HPO_4{\cdot}7H_2O$, 40 mM $NaH_2PO_4{\cdot}H_2O$, 10 mM KCL, 1 mM $MgSO_4{\cdot}7H_2O$), and the supernatants were removed. Cells were lysed by repeated freeze/thaw cycles using liquid nitrogen, and BMEZ buffer (Z buffer + 0.27% β-mercaptoethanol) was added. Reactions were started with the addition of o-nitrophenyl-β-D-galactoside dissolved in Z buffer and incubated at 30° for the duration of the experiment. Reactions were stopped by the addition of Na_2CO_3 and absorbance readings at OD_{420} were measured and used to calculate β-galactosidase units. A minimum of four replicates was performed for each strain.

Nucleotide excision repair assays

Yeast cells were grown in YPD liquid media to an OD_{600} of ~0.6. After removing a "no UV" control aliquot, the YPD medium was removed and the cells were resuspended in water and subsequently irradiated with 100 J/m^2 of UV light (time "0"). Cells were resuspended in YPD and incubated at 30° with continuous shaking. Aliquots were spun down and placed in the −80° freezer at the indicated time points. Cells were lysed by bead beating, and DNA was extracted as described (Rose *et al.* 1990). DNA was resuspended in T4 endonuclease reaction buffer to a final concentration of 4 mM Tris (pH 7.4), 2 mM EDTA, 25 mM NaCl, and 25 μg/mL BSA in the presence or absence of T4 endonuclease V (Epicentre) for a minimum of 2 hr at 37°. Afterward, single-strand DNA was resolved on a 1.2% alkaline gel and stained with SYBR Gold (Invitrogen). The gel was scanned by Typhoon FLA 7000 (GE Healthcare), and quantifications were performed using ImageQuant 5.2 (Molecular Dynamics) to determine the number of CPDs per kilobase as previously described (Bespalov *et al.* 2001).

Base excision repair assays

Repair assays were conducted as previously described (Czaja *et al.* 2010). Briefly, yeast cells were grown in YPD to an OD_{600} of ~0.6. After removing a "no MMS" control aliquot, cultures were treated with 0.2% MMS (Sigma) for 10 min. Cells were washed with water and resuspended in YPD (time "0"). Cells were allowed to repair for indicated periods of time at 30° with continuous shaking, harvested, and frozen at −80°. Cells were lysed by bead beating and DNA was

extracted as described (Rose *et al.* 1990). DNA was resuspended in MOPS buffer (70 mM MOPS pH 7.5, 1 mM DTT, 1 mM EDTA, 5% glycerol) with or without alkyladenine DNA glycosylase (AAG, from Leona Samson, Massachusetts Institute of Technology) and APE1 endonuclease (NEB) for a minimum of 2 hr. These and undigested controls were run on a 1.2% alkaline agarose gel to resolve single-stranded DNA and stained with SYBR Gold (Invitrogen). The gel was scanned by Typhoon FLA 7000 (GE Healthcare), and removal of lesions was quantified using ImageQuant 5.2 (Molecular Dynamics) and analyzed using previously published quantification methods. Data are given as the percentage of lesions removed compared to the "0" time point for three independent replicate experiments.

Chromatin immunoprecipitation

Chromatin immunoprecipitation (ChIP) was conducted and analyzed using a modified version of previously published protocols (Kyriss *et al.* 2010; Zheng *et al.* 2010). Briefly, yeast cells were grown to an OD_{600} of 0.6–0.8 and cross-linked using 1% formaldehyde (v/v). Cells were lysed by bead beating at 4°, and chromatin was sonicated using a Bioruptor (Diagenode) to create chromatin fragments averaging ~500 bp. Chromatin extract was immunoprecipitated using an anti-FLAG antibody (Sigma) bound to magnetic beads. The immunoprecipitated and input chromatin were proteinase K (Thermo) digested, cross-links were reversed, and DNA was phenol-chloroform-extracted and ethanol-precipitated. After treating with RNAse A (Thermo), the DNA was analyzed by quantitative PCR (qPCR). qPCR experiments were conducted using EvaGreen qPCR master mix (Biotium) and the ABI 7500 Fast Real-Time PCR system using region specific primers. Data are given as the percentage immunoprecipitated compared to input whole-cell extract, representing at least three replicates (except for Figure S6; see legend). Primer sequences are available upon request.

Western blot analysis of yeast extracts

Yeast strains were grown to mid-log phase and proteins were extracted using 0.1% NaOH. Blots were probed using 1:3000 dilution of anti-H2A (ActiveMotif catalog no. 39235), 1:3000 dilution of anti-H2B (ActiveMotif catalog no. 39237), 1:1000 dilution of anti-H3 (ActiveMotif catalog no. 39163), or 1:1000 dilution of anti-H3K36me3 (Abcam catalog no. ab9050) primary antibody followed by 1:3000 dilution of anti-rabbit (Bio-Rad catalog no. 172-1019) secondary. Anti-GAPDH antibody (Thermo Scientific catalog no. MA5-15738) was used as a loading control using an anti-mouse (Bio-Rad catalog no. 170-6516) secondary. Blots were imaged using a Typhoon FLA 7000 (GE Healthcare) and analyzed using ImageQuant 5.2 software.

Microarray data and analysis

Microarray experiments were performed as previously described (Kyriss *et al.* 2010) with slight modifications. Triplicate yeast cultures for the wild-type and H2A R78A mutant strains were grown to mid-log phase in YPD media at 30° and harvested. Total RNA was isolated by hot acid phenol–chloroform extraction and used for microarray analysis following standard Affymetrix protocols for Yeast Genome 2.0 GeneChip arrays.

Microarray data were processed using the MAS 5.0 algorithm implemented in the Bioconductor R package (Gentleman *et al.* 2004) after removing data from probes for *Schizosaccharomyces pombe* transcripts using published methods (Gillespie *et al.* 2010). Differentially expressed genes were identified using the limma R package (Smyth 2005), using a Benjamini–Hochberg adjusted *P*-value threshold of 0.05 and fold-change threshold of 1.7 (up or down), as previously described (Van Wageningen *et al.* 2010; Lenstra *et al.* 2011). Genes up-regulated in the H2A R78A mutant were analyzed for enriched chromatin features using the ChromatinDB database (O'Connor and Wyrick 2007).

Results

Effects of histone sprocket arginine mutants on cell growth, gene repression, and cryptic transcription

To characterize the biological functions of sprocket arginine residues, we constructed alanine mutations in each of the histone arginine residues that insert into the DNA minor groove (*i.e.*, H4 R45A, H3 R63A, H3 R83A, H2A R43A, H2B R36A, H2A R78A, and H3 R49A; see Figure 1A). Each sprocket arginine mutant was constructed in the same plasmid (pQQ18) (Ahn *et al.* 2005), which contains genes coding for each of the four core histone proteins (*HTA1*, *HTB1*, *HHT2*, *HHF2*) under the control of their native promoters. Using this strategy, we were able to introduce each histone mutant into a common yeast strain background (JHY205) (Ahn *et al.* 2005) and thus directly compare phenotypes for mutants in each of the four core histone genes. While the H4 R45A mutant was lethal, in accordance with previous reports (Matsubara *et al.* 2007; Dai *et al.* 2008; Nakanishi *et al.* 2008), the other sprocket arginine mutants were viable (Figure 1, B and C). Additionally, the viable histone sprocket arginine mutants were expressed at roughly wild-type levels based on Western blot analysis of yeast whole-cell extracts (Figure S1).

We first examined the role of sprocket arginine residues in regulating yeast gene expression. Mutations in H4 R45 were originally isolated in a genetic screen for mutants that enabled expression of an *HO-lacZ* reporter gene in the absence of a functional SWI/SNF complex (Kruger *et al.* 1995). In our strain background, we confirmed that the H4 R45A mutant (in the presence of wild-type H2A; see legend for Figure 2) significantly induced expression of the *HO-lacZ* reporter in the *snf5Δ* mutant background (Figure 2A), as judged by LacZ activity assays. Significant increases in LacZ expression were also detected for the H3 R63A and H3 R49A mutants, although the magnitude of the increase was considerably smaller in these mutants (Figure 2A). Intriguingly, the H3 R49A mutant also significantly increased expression of the *HO-lacZ* reporter in the *SNF5* wild-type

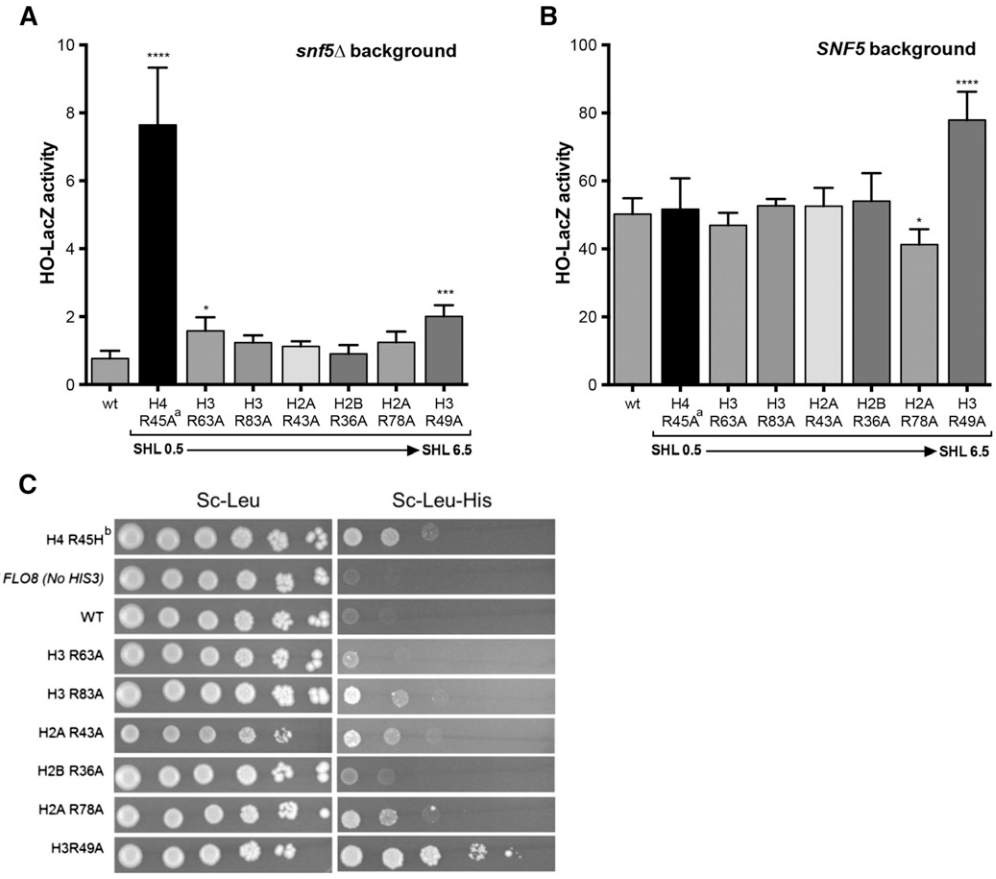

Figure 2 Effects of histone sprocket arginine mutants on expression of the *HO-lacZ* reporter and cryptic transcription of the *FLO8-HIS3* reporter. (A) LacZ activity was measured for extracts from each histone mutant strain in a *snf5Δ* genetic background. Mean and standard deviation of LacZ activity from at least three independent experiments is depicted for each strain. The SHLs of nucleosomal DNA bound by each arginine residue are indicated. *P*-values were corrected for multiple hypothesis testing. $^{****}P < 0.0001$; $^{***}P < 0.001$; $^{**}P < 0.01$; $^{*}P < 0.05$. [a]The H4 R45A mutant strain also contains the wild-type (wt) histone H4 gene. (B) Same as in A, except the strains are wild type for *SNF5*. (C) Yeast strains containing the *FLO8-HIS3* reporter (excepting the wild-type *FLO8* control) were spotted at decreasing serial dilutions on SC-LEU and SC-LEU-HIS plates. Growth on SC-LEU-HIS plates indicates activation of the *FLO8* cryptic transcript containing the *HIS3* reporter. [b]The H4 R45H mutant strain also contains the wild type (wt) histone H4 gene.

background (Figure 2B). In contrast, the H4 R45A mutant had no effect on *HO-lacZ* expression in *SNF5* wild-type cells, indicating that these two sprocket arginine mutants likely affect *HO-lacZ* expression via distinct mechanisms.

We also examined the effects of the sprocket arginine residues on cryptic intragenic transcription. Previous studies have discovered that the H3 R49A sprocket arginine mutant activates transcription initiation from a cryptic promoter within the *FLO8*-coding sequence due to a defect in Set2-dependent H3 K36 methylation (Hainer and Martens 2011). We tested the effects of this and other sprocket arginine mutants on *FLO8* cryptic transcription using a *FLO8-HIS3* reporter (Cheung *et al.* 2008) and scoring for growth on media lacking histidine (SC-Leu-His; see Figure 2C). We confirmed that the H3 R49A mutant induced cryptic transcription from the *FLO8-HIS3* reporter, enabling the strain to grow in media lacking histidine. In contrast, essentially no growth was detected on media lacking histidine for the wild-type strain (Figure 2C). We found that multiple sprocket arginine mutants induced *FLO8* cryptic transcription, namely H3 R83A, H2A R43A, H2A R78A, and H4 R45H (Figure 2C), although apparently to a lesser extent than the H3 R49A mutant. Unlike H3 R49A, however, these other sprocket arginine mutants do not affect H3 K36 trimethylation (Figure S2), indicating that they regulate cryptic transcription through a distinct pathway. In summary, the H4 R45 and H3 R49 residues regulate HO repression but through distinct mechanisms, and multiple sprocket arginine residues are required to repress cryptic transcription.

H3 R49 and H2A R78 sprocket arginine residues are required for efficient nucleotide excision repair of UV-induced DNA lesions

We next examined the role of sprocket arginine residues in DNA repair. Yeast cells with mutations in the H4 R45 sprocket arginine have the unusual phenotype of being more resistant to UV radiation, likely because the cells more efficiently repair UV-induced DNA lesions (Nag *et al.* 2008). We found that none of the other sprocket arginine mutants were more resistant to killing by UV radiation (Figure S3); however, the H2A R78A and H3 R49A sprocket arginine mutants were significantly more sensitive to UV radiation than wild-type cells in our strain background (Figure S3 and Figure 3A).

We tested whether the increased UV sensitivity in these mutants was due to a defect in NER by measuring the repair of CPDs, a major class of UV-induced DNA lesions that is repaired by the NER pathway, in the histone mutant cells following UV exposure. We observed a significant global defect in the repair of CPDs in the H2A R78A and H3 R49A mutants relative to wild type (Figure 3, B and D). Both mutants had a very similar defect in NER efficiency (and

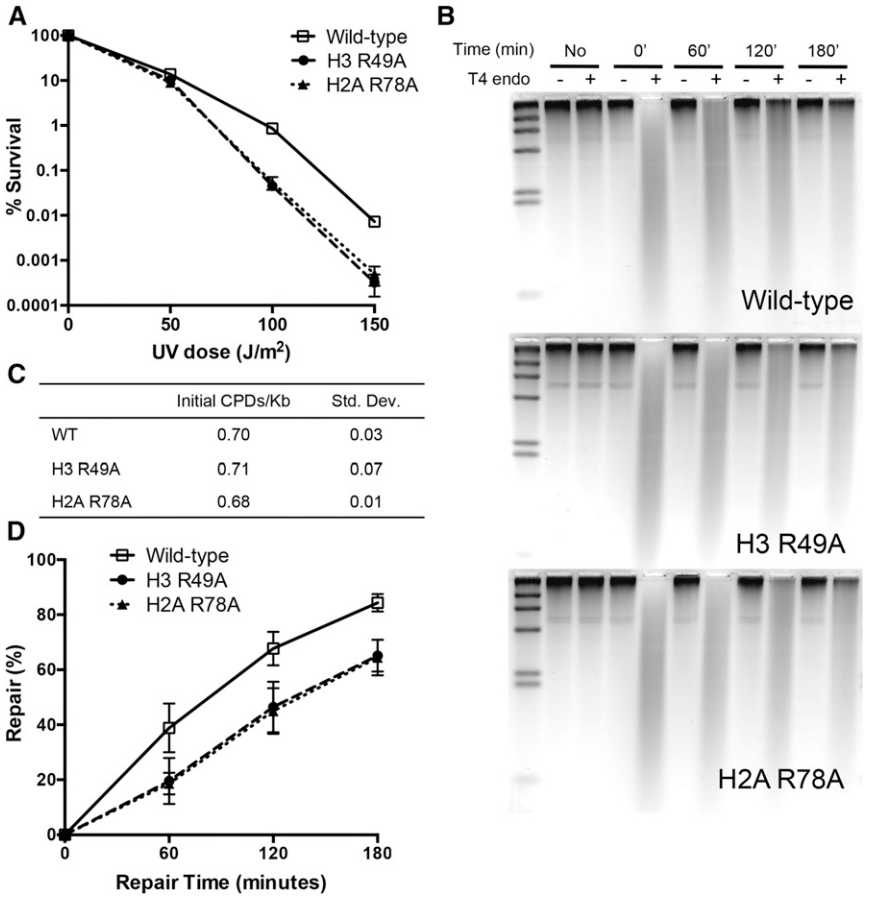

Figure 3 H3 R49 and H2A R78 histone residues are required for survival and efficient NER of UV-induced DNA lesions. (A) UV survival assays of histone mutant strains. (B) Representative alkaline gels from genomic NER assays of histone mutants. Genomic DNA was isolated from yeast cells before UV exposure or at the indicated time points following UV radiation (100 J/m^2). Isolated genomic DNA was treated with or without T4 endonuclease, which makes single-stranded DNA (ssDNA) nicks at sites of UV-induced CPDs. (C) Quantification of initial frequency of CPDs per kilobase of genomic DNA. (D) Quantification of the percentage of repair of CPDs from alkaline gels. Mean and standard deviation of the percentage of repair of CPDs from three independent experiments is depicted.

UV sensitivity), but neither mutant significantly altered the initial CPD damage levels following UV exposure (Figure 3C). These data indicate that sprocket arginine residues that bind near the ends of the nucleosomal DNA function in NER.

H2A R78A sprocket arginine residue does not affect basal expression of NER genes, but is required for gene repression

One possible explanation for the observed NER defects is that the histone mutants may reduce the expression of one or more key NER genes. We tested this possibility by measuring genome-wide expression changes in the H2A R78A mutant relative to wild type using Affymetrix microarrays. Importantly, we observed no significant decreases in the expression of any NER genes under normal growth conditions (Table S3).

Overall, 290 genes showed an increase in messenger RNA (mRNA) levels, and only 8 genes showed a decrease in mRNA levels in the H2A R78A mutant strain. Gene ontology analysis using the FunSpec software (Robinson *et al.* 2002) revealed that the up-regulated genes were enriched for the sporulation ($P = 3.8 \times 10^{-10}$), oxidation-reduction ($P = 2.2. \times 10^{-8}$), and carbohydrate metabolism ($P = 5.2 \times 10^{-7}$) functional categories. Because the H2A R78A mutant induced cryptic transcription of the *FLO8-HIS3* reporter gene (see Figure 2C), it is possible that some of the gene expression changes could reflect activation of cryptic transcripts. However, we did not observe a significant enrichment of yeast genes with known cryptic transcripts (Cheung *et al.* 2008). Analysis of histone occupancy ChIP-chip data in ChromatinDB (O'Connor and Wyrick 2007) indicated that the 290 up-regulated genes had higher levels of histone occupancy in their promoter regions in wild-type cells and were depleted for permissive chromatin marks (Figure S4). Taken together, these data suggest that the H2A R78 sprocket arginine is required for chromatin-mediated repression of many yeast genes.

Histone sprocket arginine mutants are sensitive to MMS but do not affect base excision repair

Many of the sprocket arginine mutants are sensitive to MMS, a DNA-damaging agent that generates alkylated base lesions that are primarily repaired by the BER pathway. We confirmed the MMS sensitivity of the H3 R83A, H2A R43A, H2A R78A, and H3 R49A mutants in our strain background (Figure 4A). As two of these mutants showed an NER defect, we tested each MMS-sensitive strain for a possible defect in BER by measuring the repair of the two major MMS-induced DNA lesions, 3-methyladenine and 7-methylguanine. However, we found that none of these histone mutants caused a global defect in BER (Figure 4, B–D),

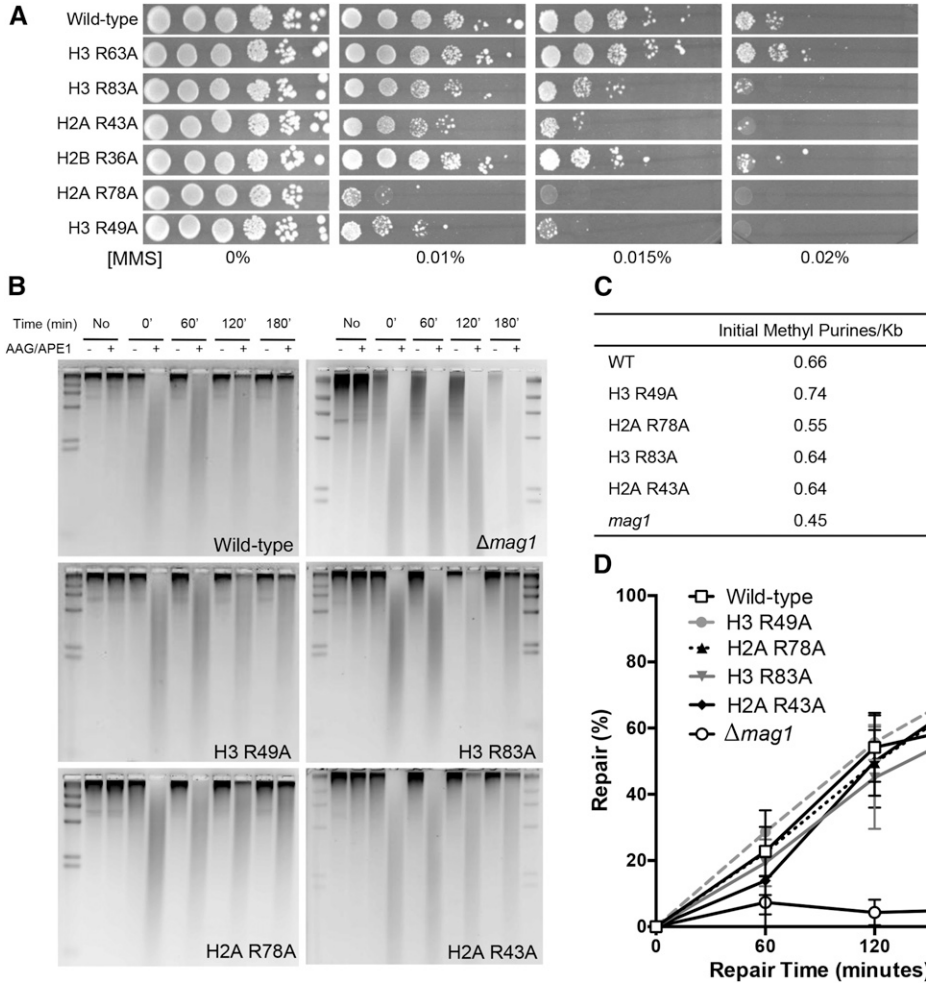

Figure 4 Histone sprocket arginine mutants are sensitive to MMS, but do not affect BER efficiency of MMS-induced DNA lesions. (A) Sprocket arginine mutant strains were spotted at decreasing serial dilutions on plates containing the indicated doses of MMS. (B) Representative alkaline gels from genomic BER assays of histone mutants and a *Δmag1* control strain. DNA was isolated from yeast cells before MMS exposure or at the indicated time points following MMS treatment (0.2% for 10 min). Isolated genomic DNA was treated with (or without) AAG/APE1 to induce ssDNA nicks at sites of 3-methyladenine and 7-methylguanine lesions. (C) Quantification of initial frequency 3-methyladenine and 7-methylguanine lesions per kilobase of genomic DNA. (D) Quantification of the percentage of repair of MMS-induced DNA damage from alkaline gels. Mean and standard deviation of the percentage of repair from three independent experiments is depicted.

indicating that the MMS sensitivity is likely not due to a global deficiency in repairing these base lesions.

Double mutants of adjacent sprocket arginine residues near the DNA exit/entry sites are lethal

While our data clearly indicate that multiple sprocket arginine residues have important roles in transcription and DNA repair (particularly H2A R78 and H3 R49), only the H4 R45 sprocket arginine residue is essential for cell viability (Figure 1B). We hypothesized that the H4 R45A mutant is lethal because it is the only sprocket arginine mutant that affects DNA interactions at adjacent superhelical locations (SHL +0.5 and SHL −0.5). To test our hypothesis, we constructed double mutants of nonessential sprocket arginine residues that contacted adjacent DNA superhelical locations [*e.g.*, SHL ±1.5 (H3 R63) and SHL ±2.5 (H3 R83)]. While a number of double-mutant combinations are viable in yeast, the H2A R78A-H2B R36A and H2A R78A-H3 R49A double mutants are lethal (Figure 5A). Intriguingly, these sprocket arginine residues contact the DNA at superhelical locations near the DNA exit/entry sites in the nucleosome (Figure 1A). In contrast, double mutants of sprocket arginine residues that contact the DNA at superhelical locations distal from the exit/entry sites (*i.e.*, SHL ±1.5, SHL ±2.5, SHL ±3.5) are viable (Figure 5A), although the H3 R83A-H2A R43A and H2A R43A-H2B R36A double mutants show increased sensitivity to MMS (data not shown).

To investigate the mechanism for lethality, we constructed a yeast strain expressing the H2A R78A-H2B R36A double mutant under the control of the endogenous histone promoter and wild-type H2A and H2B under the control of the heterologous *GAL1* promoter. This strain was viable in galactose media, as the wild-type H2A and H2B genes were expressed at high levels. Wild-type H2A and H2B expression was shut off when shifted to glucose media, permitting us to better characterize the lethal phenotype of the H2A R78A-H2B R36A double mutant.

We first used this experimental system to test the growth rates of various control histone mutants following the shutoff of wild-type H2A and H2B expression in glucose media. Strains containing the H2A R78A or H2B R36A single mutants grew similar to wild type after the shift to glucose media, eventually reaching stationary phase (Figure 5B). In contrast, an H2A L1 loop deletion (H2A Δ39-42) mutant, which presumably cannot fold or assemble into the nucleosome, arrested in growth about as rapidly as the

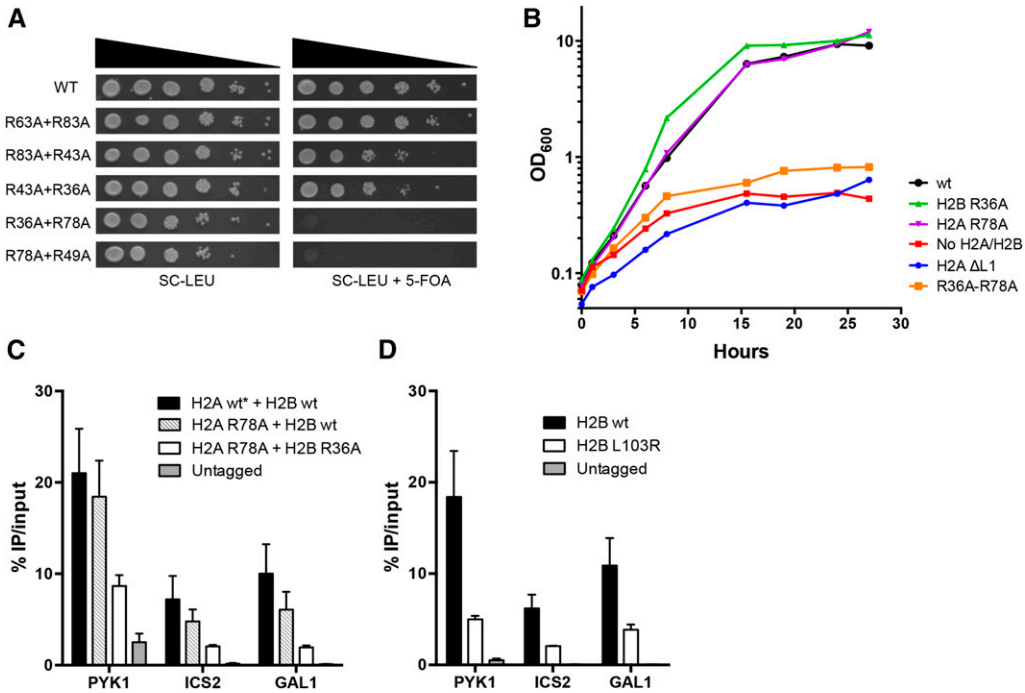

Figure 5 The histone H2A R78A-H2B R36A double mutant causes a rapid cessation of cell growth and a defect in histone occupancy. (A) Yeast strains containing the indicated double mutants were spotted as described in Figure 1B. (B) Growth rate of histone mutants upon repression of wild-type histone H2A and H2B genes by shifting to glucose media ("0" hour). The H2A ΔL1 strain has a deletion in the essential L1 loop (residues 39–42). (C) Histone occupancy of the FLAG-tagged wild-type or mutant histone H2B in the indicated genetic background (see text for more details) was measured by ChIP at select genomic regions. *Strain contained wild-type H2A and H2A R78A mutant. (D) Same as in C using a FLAG-tagged wild-type H2B or mutant H2B L103R.

"no H2A/H2B" control. The H2A R78A-H2B R36A double mutant typically arrested in growth after the shift to glucose media with kinetics similar to both the H2A L1 loop deletion and the "no H2A/H2B" controls (Figure 5B). These data suggest that the double mutant may not be able to properly assemble into nucleosomes.

H2A R78A-H2B R36A double mutant causes a defect in histone occupancy in vivo

To test this hypothesis directly, we used ChIP to measure the incorporation of the H2A R78A-H2B R36A double-mutant dimer in chromatin. Since the double mutant is lethal, we constructed a strain that is homozygous for the H2A R78A mutation and expresses both a FLAG-tagged H2B R36A mutant gene and an untagged wild-type H2B gene (strain YAH013; see Table S1). This strain was viable due to the presence of the untagged H2B wild-type gene, and all H2B-FLAG-containing dimers contained the H2A R78A-H2B R36A double mutation. Western blot analysis indicated that the FLAG-tagged H2B protein was expressed at only slightly reduced levels as compared to untagged wild-type H2B (Figure S5A). We performed ChIP-qPCR experiments on this strain using an anti-FLAG antibody to measure the incorporation and occupancy of the double-mutant dimer (*i.e.*, H2A R78A-H2B R36A) at four well-characterized genomic loci: the promoter of *ICS2*, the 5′-coding regions of *PYK1* and *GAL1*, and the 3′-coding region of *PMA1*. The *PMA1* primer set had high background signal in a few of the untagged control experiments, so we focused on the first three genomic regions for our analysis.

ChIP analyses indicated that the H2A R78A-H2B R36A double-mutant dimer was incorporated into chromatin as its occupancy was significantly greater than the untagged control at each of the three genomic regions tested (Figure 5C and Figure S5B). However, the occupancy of the H2A R78A-H2B R36A double-mutant dimer was decreased compared to wild type or the H2A R78A mutant alone (Figure 5C). In contrast, the H2A R78A mutant alone caused a marginal decrease in H2B occupancy that was not significantly different from wild type (Figure 5C; $P > 0.05$). Similar results were obtained using FLAG-tagged H2A strains for the ChIP experiments (Figure S6A) although the decrease in H2A occupancy in the double mutant was statistically significant only at the *GAL1* 5′-coding region ($P < 0.05$). A caveat is the H2A-FLAG protein did not express well in our strain background (Figure S6B).

The ChIP data indicate that the H2A R78A-H2B R36A double mutant can be assembled into chromatin *in vivo*, but this assembly is less efficient (or less stable) than wild-type H2A-H2B. For comparison, we used ChIP to measure the decrease in H2B occupancy in the H2B L103R mutant, which partially disrupts the binding of the H2A-H2B dimer to the nucleosome (Jamai *et al.* 2007). Interestingly, the H2B L103R mutant caused a similar decrease in histone occupancy as the H2A R78A-H2B R36A double mutant (Figure 5D), yet the H2B L103R mutant is viable (Jamai *et al.* 2007 and data not shown). In summary, these data show that the H2A R78A-H2B R36A double-mutant dimer has a defect in chromatin incorporation, but the relative magnitude of this defect suggests that it is not the primary cause of lethality.

Discussion

In this study, we have characterized the biological functions of histone sprocket arginine residues in the model eukaryote *Saccharomyces cerevisiae*. Unlike previous studies (Matsubara *et al.* 2007; Nakanishi *et al.* 2008; Sakamoto *et al.* 2009), our

study employed a common strain background for assaying the phenotypes of both histone H2A/H2B and H3/H4 mutants, which enabled us to directly compare these histone mutant phenotypes. The H4 R45 sprocket arginine residue is known to affect *HO* transcription, UV resistance, NER efficiency, and cell viability in yeast. As detailed below, we have identified novel functions for the remaining six sprocket arginines in these and other biological pathways. Our systematic analysis reveals simple rules for how the location and structural mode of DNA binding influence the biological function of each histone sprocket arginine residue.

The H4 R45 residue, which inserts into adjacent DNA minor grooves immediately flanking the dyad, is the only sprocket arginine required for cell viability. We hypothesized that the H4 R45A mutant is lethal because it is the only sprocket arginine mutant that affects DNA interactions at adjacent superhelical locations (SHL +0.5 and SHL −0.5). However, we found that double sprocket arginine mutants that affect binding to adjacent superhelical locations were in many cases viable (*i.e.*, H3 R63A-H3 R83A, H3 R83A-H2A R43A, and H2A R43A-H2B R36A). Only double mutants that affect adjacent superhelical locations near the DNA ends were lethal (*i.e.*, H2A R78A-H2B R36A and H2A R78A-H3 R49A).

We focused on investigating the mechanism of lethality in the H2A R78A-H2B R36A, since this double mutant was more amenable to study. We hypothesized that the H2A R78A-H2B R36A double mutant is lethal due to a defect in nucleosome assembly. This hypothesis is supported by data from time-course experiments that revealed that the H2A R78A-H2B R36A double mutant arrests in growth fairly rapidly after the expression of wild-type H2A-H2B is shut off. Consistent with the growth kinetics, ChIP experiments indicate that the H2A R78A-H2B R36A double mutant can be assembled into chromatin but at a significantly reduced efficiency (or stability) compared to wild-type H2A-H2B or the H2A R78A mutant alone. While this decrease in histone occupancy could potentially explain the lethal phenotype, we do not favor this hypothesis because we also found that the viable H2B L103R mutant has a similar decrease in histone H2B occupancy. Instead, our current working hypothesis is that incorporation of one double-mutant dimer (*i.e.*, a "heterozygous" nucleosome) is tolerated, but incorporation of two double-mutant dimers within a single nucleosome is destabilizing, thus leading to lethality. It is not clear if a related mechanism may be responsible for the lethality of the H2A R78A-H3 R49A double mutant.

The H4 R45 sprocket arginine residue was originally characterized in a screen for *sin* mutations that induced HO expression in the absence of the SWI/SNF chromatin-remodeling complex (Kruger *et al.* 1995). None of the other sprocket arginine residues had the same magnitude of effect on HO expression as the H4 R45 mutant, but we did observe significant changes in HO expression in a few other sprocket arginine mutants, particularly H3 R49A. A previous study did not detect a *sin* phenotype for the H3 R49A mutant in the presence of the wild-type H3 gene (Hainer and Martens 2011), indicating that the H3 R49A *sin* phenotype is likely to be recessive, unlike the original SIN histone mutants. The H3 R49A *sin* phenotype is also distinct in that it increases HO expression even when the wild-type SWI/SNF complex is present. Based on these data, we hypothesize that the H3 R49A mutant increases HO expression through a different pathway than SWI/SNF-dependent chromatin remodeling at the HO promoter. H3 R49 binds near the nucleosomal DNA exit/entry site and has been shown to affect nucleosomal DNA unwrapping *in vitro* (Ferreira *et al.* 2007). Our current model is that the H3 R49A mutant causes increased DNA unwrapping from *HO* promoter nucleosomes, which stimulates HO transcription.

An alternative hypothesis is that the H3 R49A mutant increases *HO-lacZ* expression by inducing the expression of cryptic transcripts within the *HO* locus that encode a functional LacZ protein. A previous study discovered that the H3 R49A mutant activates cryptic transcription at multiple loci (*e.g.*, *FLO8*, *STE11*, and *SYF1*) due to a defect in H3 K36 methylation (Hainer and Martens 2011). We confirmed that H3 R49A induced cryptic transcription using a *FLO8-HIS3* reporter (Cheung *et al.* 2008). Furthermore, we identified additional sprocket arginine mutants (*i.e.*, H4 R45H, H3 R83A, H2A R43A, and H2A R78A) that also activated cryptic transcription of this reporter, although to a lesser extent than was observed for the H3 R49A mutant and through a pathway distinct from H3 K36 methylation.

Mutations in the H4 R45 sprocket arginine residue also enhance UV resistance and increase NER efficiency in yeast cells, presumably by rendering the nucleosomal DNA more accessible to NER enzymes (Nag *et al.* 2008; Nag and Smerdon 2009). While none of the other sprocket arginine mutants significantly enhance UV resistance, we discovered that the H2A R78A and H3 R49A mutants are more sensitive to UV damage and have a significant defect in NER. While the H4 R45 residue contacts DNA near the dyad center, the H3 R49 and H2A R78 residues bind near the ends of the nucleosomal DNA. These observations suggest that the translational position of the nucleosomal DNA bound by the sprocket arginine residue (*i.e.*, near dyad *vs.* near exit/entry) influences its role in UV resistance and repair.

The mechanism underlying the UV sensitivity and repair phenotypes is currently unclear. The H2A R78A and H3 R49A mutants presumably decrease the stability of DNA binding within the nucleosome, particularly near the ends of the nucleosomal DNA. A decrease in the stability of DNA binding would be expected to enhance access by NER enzymes and thus increase NER efficiency, but the opposite phenotype was observed. Moreover, there were no differences in initial damage levels in either histone mutant strain, and we further showed that the H2A R78A mutant did not decrease the basal expression of any NER genes. Recently, a number of studies have found that histone chaperones such as Spt16 and Nap1 bind to the histone surface that normally interacts with the nucleosomal DNA (D'Arcy *et al.* 2013; Hondele and Ladurner 2013; Hondele

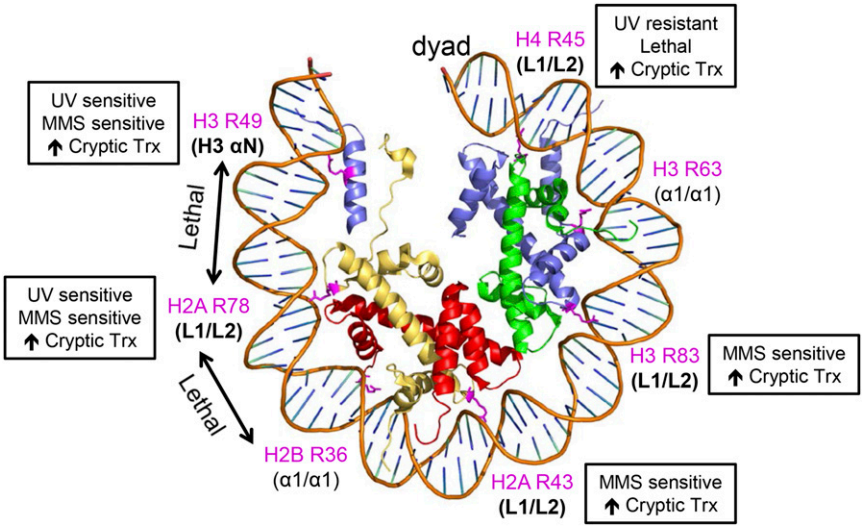

Figure 6 Translational positions of sprocket arginine residues, their associated DNA-binding motifs, and their mutant phenotypes, as identified by this study. The yeast nucleosome structure (1id3) (White *et al.* 2001) was displayed using PyMOL.

et al. 2013). For example, the H2A R78 sprocket arginine is part of the binding interface with the Spt16 Middle domain (Hondele *et al.* 2013). Hence, our current working hypothesis is that these histone mutants may be poor substrates for histone chaperones and thus may inhibit chromatin remodeling necessary for efficient NER.

Multiple sprocket arginine mutants, particularly H2A R78A and H3 R49A, were sensitive to the DNA alkylating agent MMS as anticipated from previous studies (Matsubara *et al.* 2007; Dai *et al.* 2008, 2010; Huang *et al.* 2009; Sakamoto *et al.* 2009). However, none of these mutants affected the efficiency of BER in repairing MMS-induced DNA lesions. Instead, we suspect that the MMS sensitivity may be due to a defect in DNA damage tolerance or signaling. Future studies will be needed to investigate these hypotheses.

Within the nucleosome, each histone heterodimer binds to ~27–28 bp of DNA via a central α1/α1-binding motif and two flanking Loop 1–Loop 2 (L1/L2)-binding motifs (Luger *et al.* 1997). Intriguingly, our phenotypic analysis indicates that the sprocket arginine residues located in L1/L2-binding motifs (*i.e.*, H4 R45, H3 R83, H2A R43, and H2A R78) have important roles in cryptic transcription and MMS sensitivity among other phenotypes (Figure 6). In contrast, sprocket arginine residues located in α1/α1-binding motifs (*i.e.*, H3 R63 and H2B R36) are not required for these biological processes (Figure 6) and appear to be largely dispensable.

Analysis of published data sets of histone mutant phenotypes (Matsubara *et al.* 2007; Dai *et al.* 2008; Huang *et al.* 2009; Sakamoto *et al.* 2009) largely confirms these conclusions, with two exceptions: (i) a previous study (Matsubara *et al.* 2007) did not report an MMS sensitivity for the H2A R43A mutant and (ii) the same group reported that the H3 R63A mutant was MMS sensitive (and also had HU and Spt− phenotypes) (Sakamoto *et al.* 2009). These discrepancies could be due to differences in genetic background or in the construction of the mutant strains. While we used the same genetic background for all of our sprocket arginine mutants, the other group used different strain backgrounds for the histone H2A/H2B mutants *vs.* H3/H4 mutants. Moreover, these strains likely had different relative histone dosages since either H2A-H2B or H3-H4 were expressed from a plasmid, while the remaining histones were expressed from the chromosomal loci. In contrast, all of the histone genes were expressed from the same plasmid in our strains. Interestingly, Jef Boeke's group reported results in agreement with ours (Dai *et al.* 2008; Huang *et al.* 2009), namely that the H3 R63A mutant was not sensitive to MMS (or HU) nor had any other reported phenotypes (*e.g.*, telomeric silencing, etc.). Their study used an H3 R63A mutant integrated at its chromosomal locus and thus was presumably expressed at normal levels.

In summary, our data suggest that sprocket arginine residues located in L1/L2-binding motifs tend to have more important biological functions in yeast than sprocket arginines in α1/α1-binding motifs. Moreover, L1/L2 sprocket arginine residues located near the dyad (*i.e.*, H4 R45) or near the DNA exit/entry sites (*i.e.*, H2A R78) have more severe phenotypes when mutated to alanine. It is possible that α1/α1 sprocket arginine residues have important biological functions, but these functions are masked by redundancy with other nearby histone residues. The H3 R49 sprocket arginine residue does not readily fit into this model as it is located in the H3 αN helix. H3 R49 shares many phenotypes with the adjacent H2A R78 sprocket arginine (*e.g.*, UV sensitivity, NER deficiency, MMS sensitivity, etc.), perhaps because both sprocket arginines contact the DNA near the nucleosomal DNA exit/entry sites. Hence, our data suggest that the translational position of the sprocket arginine within the nucleosome, as well as its associated binding motif, appear to strongly influence its biological function.

Acknowledgments

We thank David Allis and Linda Breeden for providing yeast strains or plasmids; Michael Smerdon and Peng Mao for helpful comments and suggestions on the manuscript; and Katie Adolphsen, Susan Kim, Anna Lindsay, Travis Ostbye,

and Russell Wilson for expert technical assistance. This work was supported by grant no. ES002614 from the National Institute of Environmental Health Sciences (NIEHS). Isaura Gallegos was supported by National Institutes of Health/National Institute of General Medical Sciences through institutional training grant award T32-GM008336. The contents are solely the responsibility of the authors and do not necessarily represent the official views of the NIEHS, NIGMS, or NIH. Microarray data for this study have been deposited in the National Center for Biotechnology Information Gene Expression Omnibus database under accession no. GSE68159.

Literature Cited

Ahn, S. H., W. L. Cheung, J. Y. Hsu, R. L. Diaz, M. M. Smith *et al.*, 2005 Sterile 20 kinase phosphorylates histone H2B at serine 10 during hydrogen peroxide-induced apoptosis in S. cerevisiae. Cell 120: 25–36.

Bespalov, V. A., A. Conconi, X. Zhang, D. Fahy, and M. J. Smerdon, 2001 Improved method for measuring the ensemble average of strand breaks in genomic DNA. Environ. Mol. Mutagen. 38: 166–174.

Cheung, V., G. Chua, N. N. Batada, C. R. Landry, S. W. Michnick *et al.*, 2008 Chromatin- and transcription-related factors repress transcription from within coding regions throughout the Saccharomyces cerevisiae genome. PLoS Biol. 6: e277.

Czaja, W., V. A. Bespalov, J. M. Hinz, and M. J. Smerdon, 2010 Proficient repair in chromatin remodeling defective ino80 mutants of Saccharomyces cerevisiae highlights replication defects as the main contributor to DNA damage sensitivity. DNA Repair (Amst.) 9: 976–984.

Dai, J., E. M. Hyland, D. S. Yuan, H. Huang, J. S. Bader *et al.*, 2008 Probing nucleosome function: a highly versatile library of synthetic histone H3 and H4 mutants. Cell 134: 1066–1078.

Dai, J., E. M. Hyland, A. Norris, and J. D. Boeke, 2010 Yin and Yang of histone H2B roles in silencing and longevity: a tale of two arginines. Genetics 186: 813–828.

D'Arcy, S., K. W. Martin, T. Panchenko, X. Chen, S. Bergeron *et al.*, 2013 Chaperone Nap1 shields histone surfaces used in a nucleosome and can put H2A–H2B in an unconventional tetrameric form. Mol. Cell 51: 662–677.

Davey, C. A., D. F. Sargent, K. Luger, A. W. Maeder, and T. J. Richmond, 2002 Solvent mediated interactions in the structure of the nucleosome core particle at 1.9 a resolution. J. Mol. Biol. 319: 1097–1113.

Ferreira, H., J. Somers, R. Webster, A. Flaus, and T. Owen-Hughes, 2007 Histone tails and the H3 alphaN helix regulate nucleosome mobility and stability. Mol. Cell. Biol. 27: 4037–4048.

Flaus, A., C. Rencurel, H. Ferreira, N. Wiechens, and T. Owen-Hughes, 2004 Sin mutations alter inherent nucleosome mobility. EMBO J. 23: 343–353.

Fry, C. J., A. Norris, M. Cosgrove, J. D. Boeke, and C. L. Peterson, 2006 The LRS and SIN domains: two structurally equivalent but functionally distinct nucleosomal surfaces required for transcriptional silencing. Mol. Cell. Biol. 26: 9045–9059.

Gentleman, R. C., V. J. Carey, D. M. Bates, B. Bolstad, M. Dettling *et al.*, 2004 Bioconductor: open software development for computational biology and bioinformatics. Genome Biol. 5: R80.

Gillespie, C. S., G. Lei, R. J. Boys, A. Greenall, and D. J. Wilkinson, 2010 Analysing time course microarray data using Bioconductor: a case study using yeast2 Affymetrix arrays. BMC Res. Notes 3: 81.

Hainer, S. J., and J. A. Martens, 2011 Identification of histone mutants that are defective for transcription-coupled nucleosome occupancy. Mol. Cell. Biol. 31: 3557–3568.

Harp, J. M., B. L. Hanson, D. E. Timm, and G. J. Bunick, 2000 Asymmetries in the nucleosome core particle at 2.5 A resolution. Acta Crystallogr. D Biol. Crystallogr. 56: 1513–1534.

Hondele, M., and A. G. Ladurner, 2013 Catch me if you can: how the histone chaperone FACT capitalizes on nucleosome breathing. Nucleus 4: 443–449.

Hondele, M., T. Stuwe, M. Hassler, F. Halbach, A. Bowman *et al.*, 2013 Structural basis of histone H2A–H2B recognition by the essential chaperone FACT. Nature 499: 111–114.

Horn, P. J., K. A. Crowley, L. M. Carruthers, J. C. Hansen, and C. L. Peterson, 2002 The SIN domain of the histone octamer is essential for intramolecular folding of nucleosomal arrays. Nat. Struct. Biol. 9: 167–171.

Huang, H., A. M. Maertens, E. M. Hyland, J. Dai, A. Norris *et al.*, 2009 HistoneHits: a database for histone mutations and their phenotypes. Genome Res. 19: 674–681.

Jamai, A., R. M. Imoberdorf, and M. Strubin, 2007 Continuous histone H2B and transcription-dependent histone H3 exchange in yeast cells outside of replication. Mol. Cell 25: 345–355.

Jin, Y., A. M. Rodriguez, J. D. Stanton, A. A. Kitazono, and J. J. Wyrick, 2007 Simultaneous mutation of methylated lysine residues in histone H3 causes enhanced gene silencing, cell cycle defects, and cell lethality in Saccharomyces cerevisiae. Mol. Cell. Biol. 27: 6832–6841.

Kruger, W., C. L. Peterson, A. Sil, C. Coburn, G. Arents *et al.*, 1995 Amino acid substitutions in the structured domains of histones H3 and H4 partially relieve the requirement of the yeast SWI/SNF complex for transcription. Genes Dev. 9: 2770–2779.

Kurumizaka, H., and A. P. Wolffe, 1997 Sin mutations of histone H3: influence on nucleosome core structure and function. Mol. Cell. Biol. 17: 6953–6969.

Kyriss, M. N., Y. Jin, I. J. Gallegos, J. A. Sanford, and J. J. Wyrick, 2010 Novel functional residues in the core domain of histone H2B regulate yeast gene expression and silencing and affect the response to DNA damage. Mol. Cell. Biol. 30: 3503–3518.

Lenstra, T. L., J. J. Benschop, T. Kim, J. M. Schulze, N. A. Brabers *et al.*, 2011 The specificity and topology of chromatin interaction pathways in yeast. Mol. Cell 42: 536–549.

Luger, K., A. W. Mader, R. K. Richmond, D. F. Sargent, and T. J. Richmond, 1997 Crystal structure of the nucleosome core particle at 2.8 Å resolution. Nature 389: 251–260.

Matsubara, K., N. Sano, T. Umehara, and M. Horikoshi, 2007 Global analysis of functional surfaces of core histones with comprehensive point mutants. Genes Cells 12: 13–33.

Muthurajan, U. M., Y. J. Park, R. S. Edayathumangalam, R. K. Suto, S. Chakravarthy *et al.*, 2003 Structure and dynamics of nucleosomal DNA. Biopolymers 68: 547–556.

Muthurajan, U. M., Y. Bao, L. J. Forsberg, R. S. Edayathumangalam, P. N. Dyer *et al.*, 2004 Crystal structures of histone Sin mutant nucleosomes reveal altered protein-DNA interactions. EMBO J. 23: 260–271.

Nag, R., and M. J. Smerdon, 2009 Altering the chromatin landscape for nucleotide excision repair. Mutat. Res. 682: 13–20.

Nag, R., F. Gong, D. Fahy, and M. J. Smerdon, 2008 A single amino acid change in histone H4 enhances UV survival and DNA repair in yeast. Nucleic Acids Res. 36: 3857–3866.

Nag, R., M. Kyriss, J. W. Smerdon, J. J. Wyrick, and M. J. Smerdon, 2010 A cassette of N-terminal amino acids of histone H2B are required for efficient cell survival, DNA repair and Swi/Snf binding in UV irradiated yeast. Nucleic Acids Res. 38: 1450–1460.

Nakanishi, S., B. W. Sanderson, K. M. Delventhal, W. D. Bradford, K. Staehling-Hampton *et al.*, 2008 A comprehensive library of histone mutants identifies nucleosomal residues required for H3K4 methylation. Nat. Struct. Mol. Biol. 15: 881–888.

O'Connor, T. R., and J. J. Wyrick, 2007 ChromatinDB: a database of genome-wide histone modification patterns for Saccharomyces cerevisiae. Bioinformatics 23: 1828–1830.

Park, J. H., M. S. Cosgrove, E. Youngman, C. Wolberger, and J. D. Boeke, 2002 A core nucleosome surface crucial for transcriptional silencing. Nat. Genet. 32: 273–279.

Parra, M. A., D. Kerr, D. Fahy, D. J. Pouchnik, and J. J. Wyrick, 2006 Deciphering the roles of the histone H2B N-terminal domain in genome-wide transcription. Mol. Cell. Biol. 26: 3842–3852.

Robinson, M. D., J. Grigull, N. Mohammad, and T. R. Hughes, 2002 FunSpec: a web-based cluster interpreter for yeast. BMC Bioinformatics 3: 35.

Rohs, R., S. M. West, A. Sosinsky, P. Liu, R. S. Mann *et al.*, 2009 The role of DNA shape in protein-DNA recognition. Nature 461: 1248–1253.

Rose, M. D., F. Winston, and P. Hieter, 1990 *Methods in Yeast Genetics: A Laboratory Course Manual*. Cold Spring Harbor Laboratory Press, Cold Spring Harbor, NY.

Sakamoto, M., S. Noguchi, S. Kawashima, Y. Okada, T. Enomoto *et al.*, 2009 Global analysis of mutual interaction surfaces of nucleosomes with comprehensive point mutants. Genes Cells 14: 1271–1330.

Smyth, G. K., 2005 Limma: linear models for microarray data, pp. 397–420 in *Bioinformatics and Computational Biology Solutions Using R and Bioconductor*, edited by R. Gentleman, V. Carey, S. Dudoit, R. Irizarry, and W. Huber, Springer, New York.

Sullivan, S. A., and D. Landsman, 2003 Characterization of sequence variability in nucleosome core histone folds. Proteins 52: 454–465.

van Wageningen, S., P. Kemmeren, P. Lijnzaad, T. Margaritis, J. J. Benschop *et al.*, 2010 Functional overlap and regulatory links shape genetic interactions between signaling pathways. Cell 143: 991–1004.

Wang, D., N. B. Ulyanov, and V. B. Zhurkin, 2010 Sequence-dependent Kink-and-Slide deformations of nucleosomal DNA facilitated by histone arginines bound in the minor groove. J. Biomol. Struct. Dyn. 27: 843–859.

Wechser, M. A., M. P. Kladde, J. A. Alfieri, and C. L. Peterson, 1997 Effects of Sin- versions of histone H4 on yeast chromatin structure and function. EMBO J. 16: 2086–2095.

West, S. M., R. Rohs, R. S. Mann, and B. Honig, 2010 Electrostatic interactions between arginines and the minor groove in the nucleosome. J. Biomol. Struct. Dyn. 27: 861–866.

White, C. L., R. K. Suto, and K. Luger, 2001 Structure of the yeast nucleosome core particle reveals fundamental changes in internucleosome interactions. EMBO J. 20: 5207–5218.

Zheng, S., J. J. Wyrick, and J. C. Reese, 2010 Novel trans-tail regulation of H2B ubiquitylation and H3K4 methylation by the N terminus of histone H2A. Mol. Cell. Biol. 30: 3635–3645.

Communicating editor: M. Hampsey

GENETICS

Supporting Information
www.genetics.org/lookup/suppl/doi:10.1534/genetics.115.175885/-/DC1

Histone Sprocket Arginine Residues Are Important for Gene Expression, DNA Repair, and Cell Viability in *Saccharomyces cerevisiae*

Amelia J. Hodges, Isaura J. Gallegos, Marian F. Laughery, Rithy Meas, Linh Tran, and John J. Wyrick

DOI: 10.1534/genetics.115.175885

SUPPLEMENTAL MATERIAL

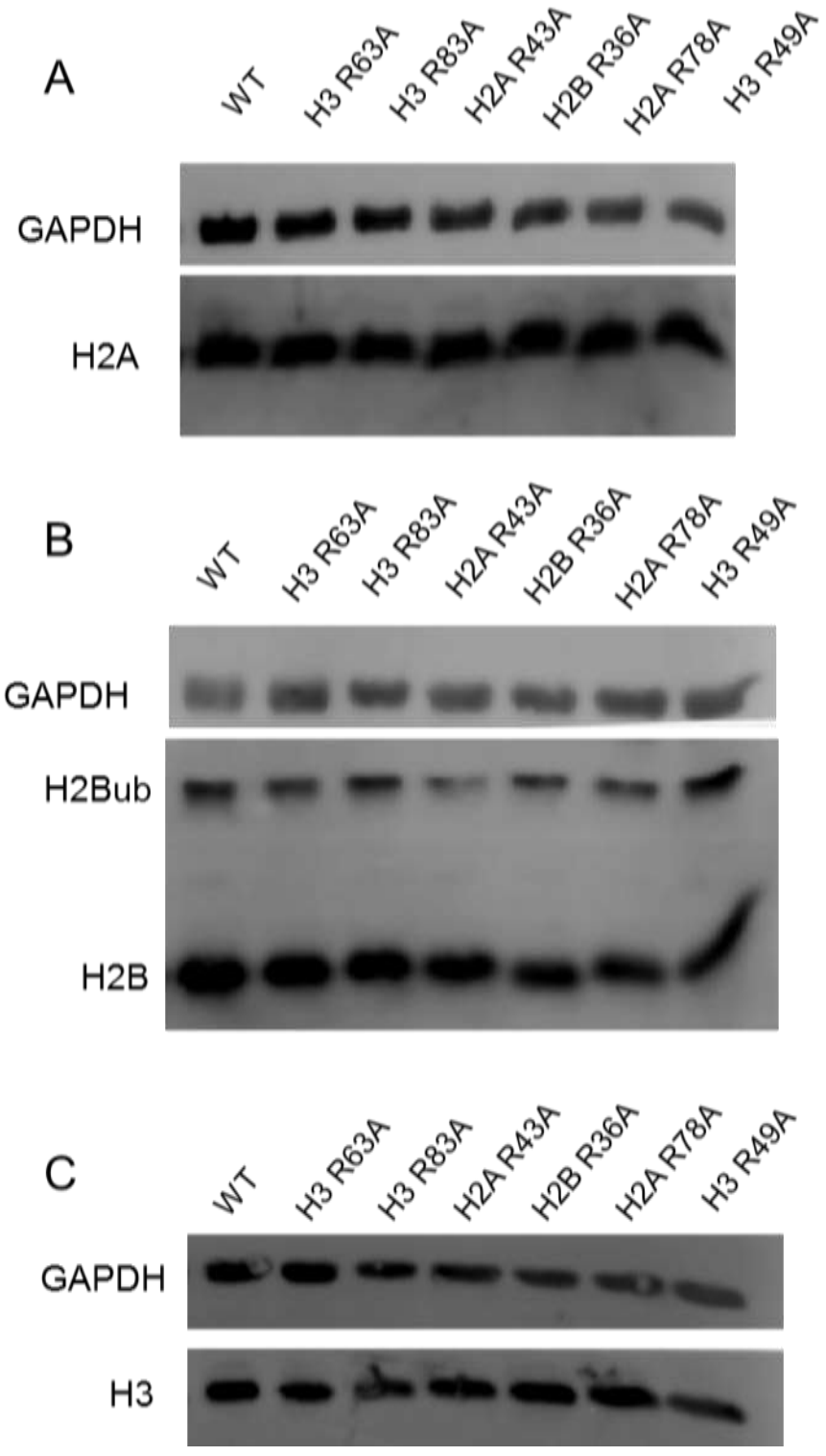

Figure S1. Histone expression levels of viable sprocket arginine mutants. Western blots were probed using antibodies against H2A (A) H2B (B) and H3 (C). GAPDH is used as a loading control.

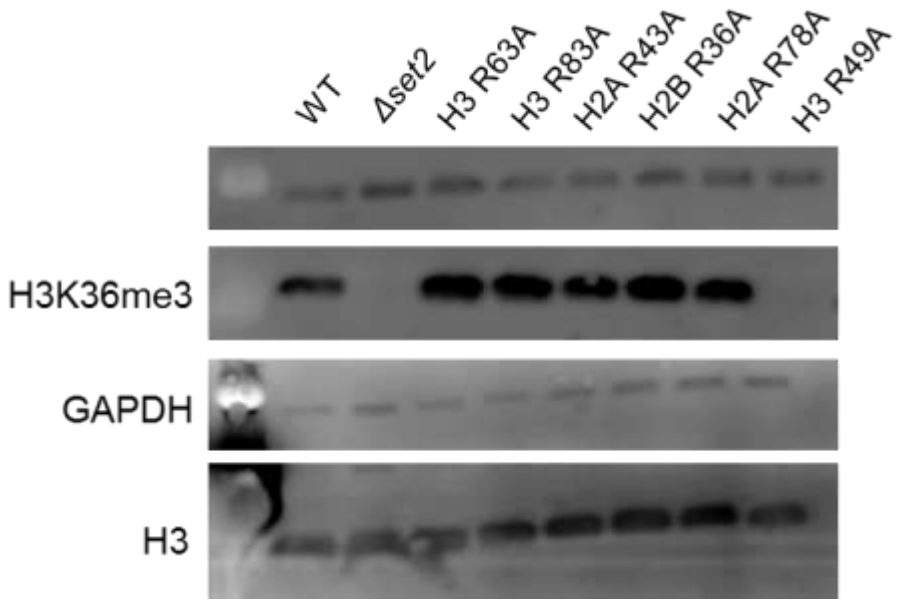

Figure S2. Methylation of H3 K36 in sprocket arginine mutants. Western blots were probed using an antibody specific for H3 K36 trimethylation or for canonical H3. GAPDH is used as a loading control.

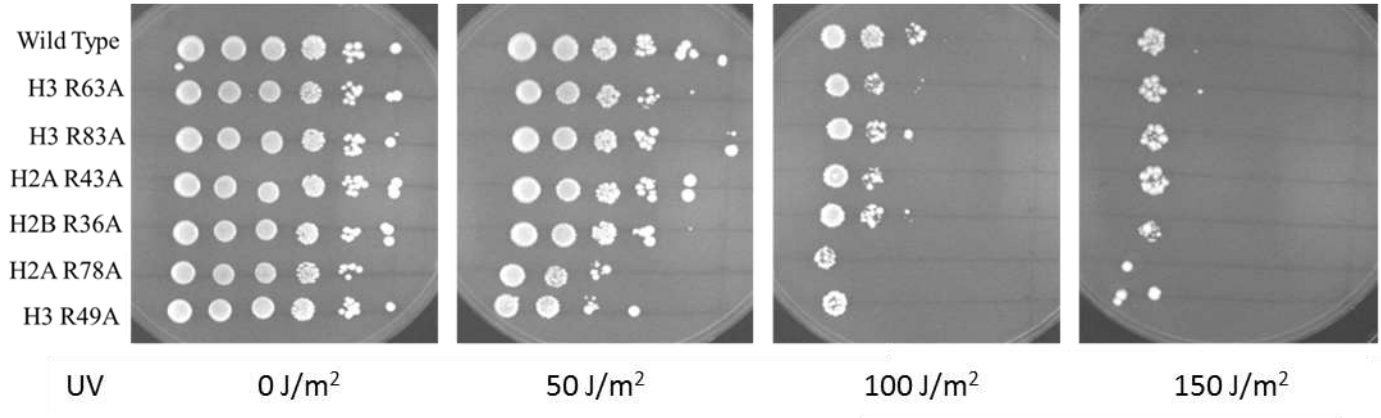

Figure S3. H3 R49A and H2A R78A sprocket arginine mutants are sensitive to UV radiation. Decreasing serial dilutions of mutant yeast cells were spot onto SC plates and exposed to the indicated doses of UV radiation.

A

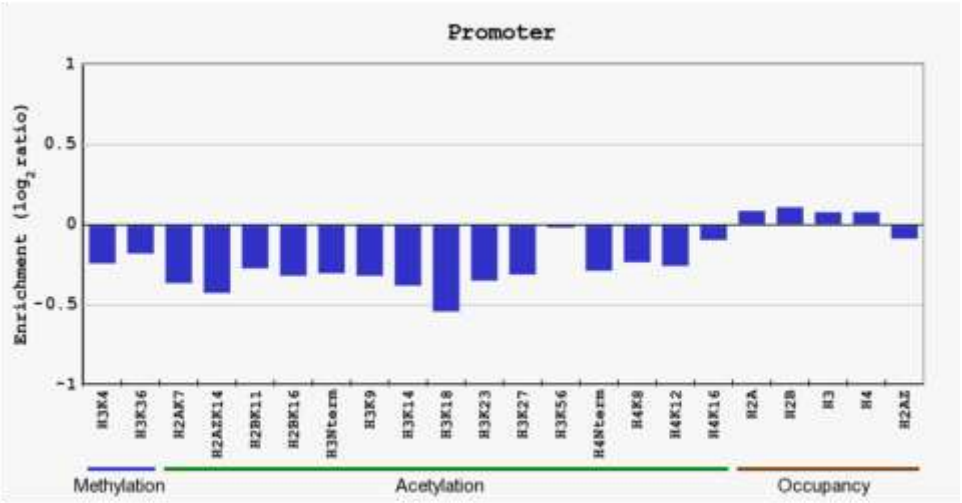

B

Chromatin Enrichment/Depletion

Promoter				
Histone Modification	Rank Percentile	Trend	P-value	Ranked Gene List
H3K4 Di-Methylation	36.9 %	**Depleted**	**$< 10^{-11}$**	
H3K36 Di-Methylation	39.2 %	**Depleted**	**$< 10^{-7}$**	
H2AK7 Acetylation	26.7 %	**Depleted**	**$< 10^{-12}$**	
H2AZK14 Acetylation	34.6 %	**Depleted**	**$< 10^{-10}$**	
H2BK11 Acetylation	27.6 %	**Depleted**	**$< 10^{-11}$**	
H2BK16 Acetylation	26.5 %	**Depleted**	**$< 10^{-12}$**	
H3Nterm Acetylation	31.0 %	**Depleted**	**$< 10^{-23}$**	
H3K9 Acetylation	29.7 %	**Depleted**	**$< 10^{-9}$**	
H3K14 Acetylation	22.7 %	**Depleted**	**$< 10^{-16}$**	
H3K18 Acetylation	23.4 %	**Depleted**	**$< 10^{-15}$**	
H3K23 Acetylation	26.4 %	**Depleted**	**$< 10^{-12}$**	
H3K27 Acetylation	30.3 %	**Depleted**	**$< 10^{-8}$**	
H3K56 Acetylation	48.6 %	none	0.5017	
H4Nterm Acetylation	29.7 %	**Depleted**	**$< 10^{-26}$**	
H4K8 Acetylation	33.9 %	**Depleted**	**$< 10^{-6}$**	
H4K12 Acetylation	29.5 %	**Depleted**	**$< 10^{-9}$**	
H4K16 Acetylation	41.4 %	none	0.0080	
H2A Occupancy	55.7 %	none	0.0065	
H2B Occupancy	61.8 %	**Enriched**	**$< 10^{-9}$**	
H3 Occupancy	62.2 %	**Enriched**	**$< 10^{-9}$**	
H4 Occupancy	61.1 %	**Enriched**	**$< 10^{-7}$**	
H2AZ Occupancy	44.0 %	none	0.0031	

Figure S4. Genes repressed by the H2A R78 sprocket arginine residue have high levels of promoter histone occupancy and low levels of active histone post-translational modifications. (A) Histone occupancy and histone modification levels in the promoter regions of 290 genes repressed by H2A R78 (i.e., genes with induced expression in the H2A R78A mutant). Analysis was performed on published ChIP-chip data sets using the web-based database ChromatinDB (O'CONNOR AND WYRICK 2007). Note, histone modification data were normalized by nucleosome occupancy levels. (B) Statistical analysis of the data shown in part A showing enrichment or depletion of histone occupancy or post-translational modifications.

.

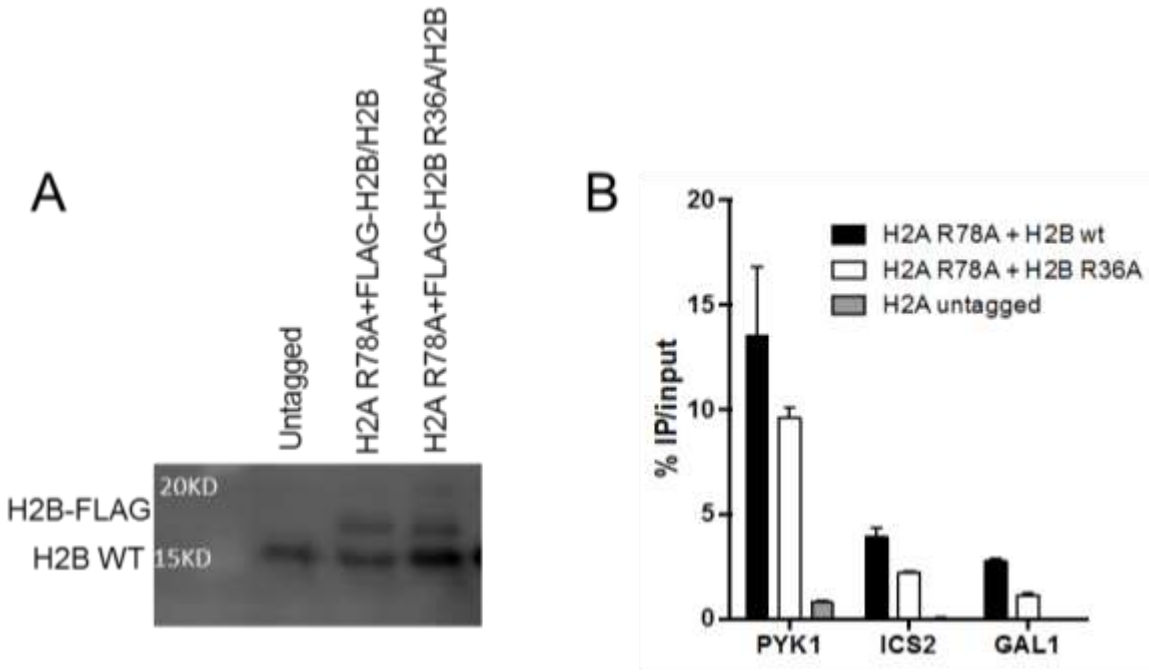

Figure S5. (A) Expression levels of wild type and FLAG-tagged H2B by western blot using an antibody against H2B. Each strain contains an untagged wild type H2B gene as well as the FLAG-tagged H2B. (B) ChIP experiments were conducted as described in Figure 5C.

.

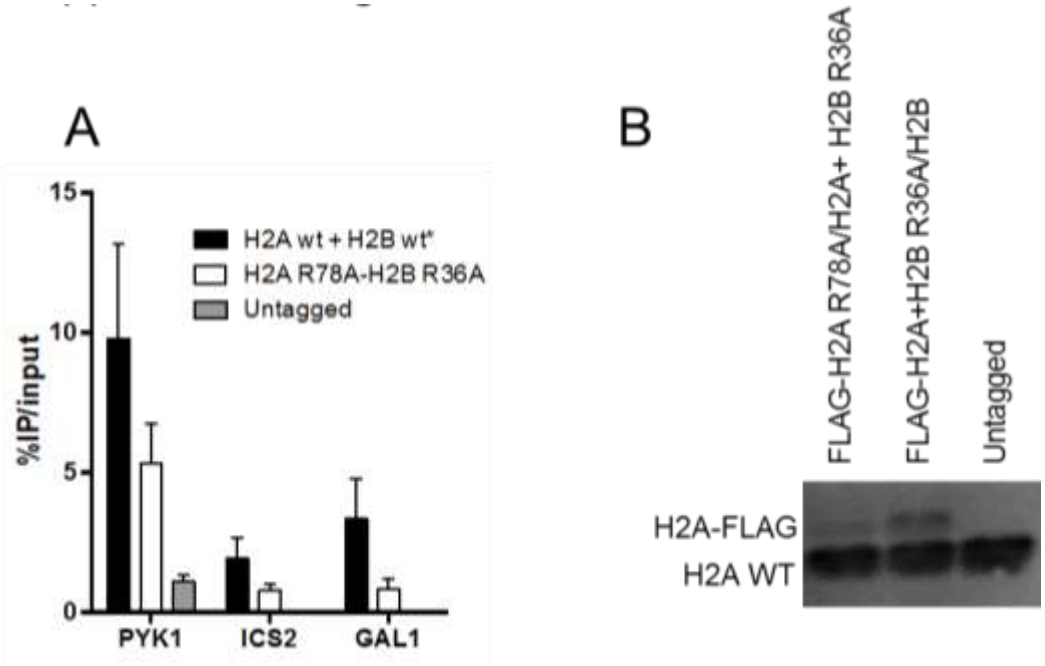

Figure S6. (A) ChIP experiments were conducted as described in Figure 5C, using a FLAG-tagged H2A. Data for the untagged control represents two independent replicates; data for wild type and mutant represents three independent replicates. *H2B wt was heterozygous for H2A R36 (B) Expression levels of wild type and FLAG-tagged H2A by western blot using an antibody against H2A.

TABLE S1. Yeast strains

Strain Name	Genotype	Used in
WY500* (WT)	*MAT**a** his3-1 leu2-0 met15-0 ura3-0 hht1-hhf1::KAN hhf2-hht2::NAT hta1-htb1::HPH hta2-htb2::NAT* p[*CEN URA3 HTA1-HTB1-HHT2-HHF2*]	Fig. 1,5
LT041 (WT snf5Δ HO-LacZ Fusion)	Isogenic to WY500, plus *snf5::HIS3 HO::LacZ*	Fig. 2
LT070 (WT snf5Δ HO-LacZ Fusion)	Isogenic to LT041; WT URA plasmid replaced with p[*CEN LEU2 HTA1-HTB1-HHT2-HHF2*]	Fig. 2
LT054 (H4 R45A +WT HO-LacZ Fusion snf5Δ)	Isogenic to LT041 plus p[*CEN LEU2 HTA1-HTB1-HHT2-hhf2_R45A*]	Fig. 2
LT063 (H3 R63A HO-LacZ Fusion snf5Δ)	Isogenic to LT041 plus p[*CEN LEU2 HTA1-HTB1-hht2_R63A-HHF2*]	Fig. 2
LT064 (H3 R83A HO-LacZ Fusion snf5Δ)	Isogenic to LT041 plus p[*CEN LEU2 HTA1-HTB1-hht2_R83A-HHF2*]	Fig. 2
LT061 H2A R43A HO-LacZ Fusion snf5Δ)	Isogenic to LT041 plus p[*CEN LEU2 hta1_R4A3-HTB1-HHT2-HHF2*]	Fig. 2
LT052 H2B R36A HO-LacZ Fusion snf5Δ)	Isogenic to LT041 plus p[*CEN LEU2 HTA1-htb1_R36A-HHT2-HHF2*]	Fig. 2
LT051 H2A R78A HO-LacZ Fusion snf5Δ)	Isogenic to LT041 plus p[*CEN LEU2 hta1_R78A-HTB1-HHT2-HHF2*]	Fig. 2
LT062 H3 R49A HO-LacZ Fusion snf5Δ)	Isogenic to LT041 plus p[*CEN LEU2 HTA1-HTB1-hht2_R49A-HHF2*]	Fig. 2
LT060 (WT SNF5 HO-LacZ Fusion)	Isogenic to WY500 plus *HO::LacZ*; WT URA plasmid replaced with p[*CEN LEU2 HTA1-HTB1-HHT2-HHF2*]	Fig. 2
LT059 (H4 R45A +WT HO-LacZ Fusion SNF5)	Isogenic to LT060 plus p[*CEN URA3 HTA1-HTB1-HHT2-HHF2] p*[*CEN LEU2 HTA1-HTB1-HHT2-hhf2_R45A*]	Fig. 2
LT067 H3 R63A HO-LacZ Fusion SNF5)	Isogenic to LT060 plus p[*CEN LEU2 HTA1-HTB1-hht2_R63A-HHF2]*	Fig. 2
LT068 (H3 R83A HO-LacZ Fusion SNF5)	Isogenic to LT060 plus p[*CEN LEU2 HTA1-HTB1-hht2_R83A-HHF2]*	Fig. 2
LT065 H2A R43A HO-LacZ Fusion SNF5)	Isogenic to LT060 plus p[*CEN LEU2 hta1_R43A-HTB1-HHT2-HHF2]*	Fig. 2
LT057 H2B R36A HO-LacZ Fusion SNF5)	Isogenic to LT060 plus p[*CEN LEU2 HTA1-htb1_R36A-HHT2-HHF2*]	Fig. 2

LT056 H2A R78A HO-LacZ Fusion SNF5)	Isogenic to LT060 plus p[*CEN LEU2 hta1_R78A-HTB1-HHT2-HHF2*]	Fig. 2
LT066 H3 R49A HO-LacZ Fusion SNF5)	Isogenic to LT060 plus p[*CEN LEU2 hta1_R78A-HTB1-hht2_R49A-HHF2*]	Fig. 2
WY504 (IJ400) (WT)	Isogenic to WY500; URA plasmid replaced with p[*CEN LEU2 HTA1-HTB1-HHT2-HHF2*]	Fig. 2,3,4, S1, S2, S3, S4
YAH034 (WT Flo8-His3 Fusion)	Isogenic to WY500 plus *FLO8::HIS3;* URA plasmid replaced with p[*CEN LEU2 HTA1-HTB1-HHT2-HHF2*]	Fig. 2
YEW2 (H4 R45H Flo8-HIS3 Fusion)	Isogenic to YAH034; URA plasmid replaced with p[*CEN LEU2 HTA1-HTB1-HHT2-hhf2_R45H*]	Fig. 2
YAH035 (H3 R63A Flo8-HIS3 Fusion	Isogenic to YAH034; URA plasmid replaced with p[*CEN LEU2 HTA1-HTB1-hht2_R63A-HHF2*]	Fig. 2
YAH036 (H3 R83A Flo8-HIS3 Fusion)	Isogenic to YAH034; URA plasmid replaced with p[*CEN LEU2 HTA1-HTB1-hht2_R83A-HHF2*]	Fig. 2
YAH037 (H2A R43A Flo8-HIS3 Fusion	Isogenic to YAH034; URA plasmid replaced with p[*CEN LEU2 hta1_R43A-HTB1-HHT2-HHF2*]	Fig. 2
YAH038 (H2B R36A Flo8-HIS3 Fusion)	Isogenic to YAH034; URA plasmid replaced with p[*CEN LEU2 HTA1-htb1_R36A-HHT2-HHF2*]	Fig. 2
YAH039 (H2A R78A Flo8-HIS3 Fusion)	Isogenic to YAH034; URA plasmid replaced with p[*CEN LEU2 hta1_R78A-HTB1-HHT2-HHF2*]	Fig. 2
YAH040 (H3 R49A Flo8-HIS3 Fusion)	Isogenic to YAH034; URA plasmid replaced with p[*CEN LEU2 HTA1-HTB1-hht2_R49A-HHF2*]	Fig. 2
LT019 (H3 R49A)	Isogenic to WY500; URA replaced with p[*CEN LEU2 HTA1-HTB1-hht2_R49A-HHF2*]	Fig. 3,4, S1, S2, S3
LT023 (H2A R78A)	Isogenic to WY500; URA replaced with p[*CEN LEU2 hta1_R78A-HTB1-HHT2-HHF2*]	Fig. 3,4, S1, S2, S3, S4
LT015 (H3 R63A)	Isogenic to WY500; URA replaced with p[*CEN LEU2 HTA1-HTB1-hht2_R63A-HHF2*]	Fig. 4, S1, S2, S3
LT016 (H3 R83A)	Isogenic to WY500; URA replaced with p[*CEN LEU2 HTA1-HTB1-hht2_R83A-HHF2*]	Fig. 4, S1, S2, S3
LT017 (H2A R43A)	Isogenic to WY500; URA replaced with p[*CEN LEU2 hta1_R43A-HTB1-HHT2-HHF2*]	Fig. 4, S1, S2, S3
LT018 (H2B R36A)	Isogenic to WY500; URA replaced with p[*CEN LEU2 HTA1-htb1_R36A-HHT2-HHF2*]	Fig. 4, S1, S2, S3

WY502 (*set2Δ*)	Isogenic to WY500 plus *set2Δ::*KAN	Fig. S2
RM001.1 (*mag1Δ*)	Isogenic to WY504 plus *mag1Δ::HIS3*	Fig. 4
WY471.1 (WT Gal Shutdown ΔL1)	Isogenic to WY500; URA plasmid replaced with p[*CEN HIS3 HTA1-pGAL-HTB1-HHT2-HHF2*] p[*CEN LEU2 hta1_Δ39-42-HTB1-HHT2-HHF2*]	Fig. 5
WY471.3 (WT Gal Shutdown Leu2)	Isogenic to WY500; URA plasmid replaced with p[*CEN HIS3 HTA1-pGAL-HTB1-HHT2-HHF2*] p[*CEN LEU2*]	Fig. 5
WY471.18 (WT Gal Shutdown H2B R36A)	Isogenic to WY500; URA plasmid replaced with p[*CEN HIS3 HTA1-pGAL-HTB1-HHT2-HHF2*] p[*CEN LEU2 HTA1-htb1_R36A-HHT2-HHF2*]	Fig. 5
WY471.23 (WT Gal Shutdown H2A R78A)	Isogenic to WY500; URA plasmid replaced with p[*CEN HIS3 HTA1-pGAL-HTB1-HHT2-HHF2*] p[*CEN LEU2 hta1_R78A-HTB1-HHT2-HHF2*]	Fig. 5
WY471.31 (WT Gal Shutdown H2A R78A-H2B R36A)	Isogenic to WY500; URA plasmid replaced with p[*CEN HIS3 HTA1-pGAL-HTB1-HHT2-HHF2*] p[*CEN LEU2 hta1_R78A-htb1_R36A-HHT2-HHF2*]	Fig. 5
YAH031 (FLAG-tagged WT)	Isogenic to WY500; URA plasmid replaced with p[*CEN LEU2 hta1_R78A-HTB1-HHT2-HHF2*] p[*CEN HIS3 HTA1-FLAGtag_htb1-HHT2-HHF2*]	Fig. 5
YAH011 (WT untagged)	Isogenic to WY500; URA plasmid replaced with p[*CEN LEU2 hta1_R78A-HTB1-HHT2-HHF2*] p[*CEN HIS3 hta1_R78A-HTB1-HHT2-HHF2*]	Fig. 5, S5
YAH012 (FLAG-tagged H2B-H2A R78A)	Isogenic to WY500; URA plasmid replaced with p[*CEN LEU2 hta1_R78A-HTB1-HHT2-HHF2*] p[*CEN HIS3 hta1_R78A-FLAGtag_htb1-HHT2-HHF2*]	Fig. 5, S5
YAH013 (FLAG-tagged H2B R36A-H2A R78A)	Isogenic to WY500; URA plasmid replaced with p[*CEN LEU2 hta1_R78A-HTB1-HHT2-HHF2*] p[*CEN HIS3 hta1_R78A-FLAGtag-htb1_R36A-HHT2-HHF2*]	Fig. 5, S5
YT09 (WT untagged)	Isogenic to WY500; URA plasmid replaced with p[*CEN LEU2 HTA1-HTB1-HHT2-HHF2*] p[*CEN URA3 HTA1-HTB1-HHT2-HHF2*]	Fig. S6
YT011 (FLAG-tagged H2A R78A H2B R36A)	Isogenic to WY500; URA plasmid replaced with p[*CEN LEU2 HTA1-htb1_R36A-HHT2-HHF2*] p[*CEN URA3 FLAGtag_hta1_R78A-htb1_R36A-HHT2-HHF2*]	Fig. S6
YT012 (H2A FLAG-tagged WT*)	Isogenic to WY500; URA plasmid replaced with p[*CEN LEU2 HTA1-htb1_R36A-HHT2-HHF2*] p[*CEN URA3 FLAGtag_HTA1-HTB1-HHT2-HHF2*]	Fig. S6

*Strain WY500 is isogenic to JHY205 (AHN *et al*. 2005)

TABLE S2. Plasmids transformed into WY500 for spotting assays

Plasmid Name	**Genotype**
pJW500* (WT)	p[*CEN LEU2 HTA1-HTB1-HHT2-HHF2*]
pLT15 (H3 R63A)	p[*CEN LEU2 HTA1-HTB1-hht2_R63A-HHF2*]
pLT16 (H3 R83A)	p[*CEN LEU2 HTA1-HTB1-hht2_R83A-HHF2*]
pLT17 (H2A R43A)	p[*CEN LEU2 hta1_R43A-HTB1-HHT2-HHF2*]
pLT18 (H2B R36A)	p[*CEN LEU2 HTA1-htb1_R36A-HHT2-HHF2*]
pLT23 (H2A R78A)	p[*CEN LEU2 hta1_R78A-HTB1-HHT2-HHF2*]
pLT19 (H3 R49A)	p[*CEN LEU2 HTA1-HTB1-hht2_R49A-HHF2*]
pLT20 (H3 R63A + H3 R83A)	p[*CEN LEU2 HTA1-HTB1-hht2_R63A_R83A-HHF2*]
pLT21 (H3 R83 + H2A R43A)	p[*CEN LEU2 hta1_R43A-HTB1-hht2_R83A-HHF2*]
pLT22 (H2A R43A + H2B R36A)	p[*CEN LEU2 hta1_R43A-htb1_R36A-HHT2-HHF2*]
pLT24 (H2A R78A + H3 R49A)	p[*CEN LEU2 hta1_R78A-HTB1-hht2_R49A-HHF2*]
pLT31 (H2A R78A + H2B R36A)	p[*CEN LEU2 hta1_R78A-htb1_R36A-HHT2-HHF2*]

*Plasmid pJW500 is identical to pQQ18 (AHN *et al*. 2005)

TABLE S3. Microarray data for H2A R78A mutant

Gene Name	Fold Change
CCL1	N.S.*
KIN28	N.S.
RAD1	N.S.
RAD2	N.S.
RAD3	N.S.
RAD4	1.3
RAD7	N.S.
RAD10	N.S.
RAD14	N.S.
RAD16	1.4
RAD23	N.S.
RAD26	N.S.
RAD28	N.S.
SSL1	N.S.
SSL2	N.S.
TFB1	N.S.
TFB2	N.S.
TFB3	N.S.
TFB4	N.S.
TFB5	N.S.

*N.S.: Not Significant